NANO LETTERS



pubs.acs.org/NanoLett
Letter

# Attonewton Force Resolution Measurements with Silicon Nanospheres at the Thermal Noise Limit in Ambient-Temperature Liquids

Aleksandr Kostarev,[¶] Mohammad K. Abdosamadi,[¶] Hiroshi Sugimoto, Minoru Fujii, Anita Jannasch,* and Erik Schäffer*

Cite This: *Nano Lett.* 2025, 25, 13476−13481



**ABSTRACT:** Precise force measurements are crucial for understanding fundamental physics or nanoscale interactions, such as those of molecular machines in biology. Optical tweezers are versatile force transducers for such measurements, enabling meticulous manipulation of small particles. However, achieving high-resolution, subfemtonewton force measurements under physiological conditions remains challenging due to thermal fluctuations and instrument noise. Here, we employed an ultrastable optical tweezers setup in an isolated environment with precise temperature control, which minimized instrumental noise and enabled prolonged, low-force measurements. We utilized water-suspended, high-refractive index silicon nanospheres for improved resolution and trapping stability. Our system achieved a force resolution of ≈60 aN, with a sensitivity of 2.7 fN Hz$^{-0.5}$, allowing us to measure forces as low as 0.30 ± 0.06 fN. Our drag force measurements demonstrate the importance of optimized experimental conditions for low-force measurements, providing a robust framework for scientific investigations that require high-precision force characterization.

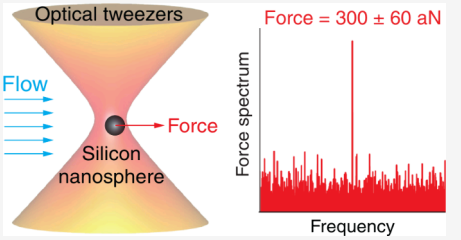


**KEYWORDS:** *Optical tweezers, attonewton resolution, silicon nanospheres, thermal noise limit, high-refractive-index nanoparticles, subfemtonewton detection*



The ability to measure small forces with high precision and accuracy is essential for understanding biological and physical processes. Piconewton optical tweezers force measurements have been widely used in biophysics to study and manipulate single molecules including motor proteins, biopolymers such as DNA, and artificial micromotors.[1−5] Some biological processes and molecules are already sensitive to subpiconewton to femtonewton forces, for example, weak molecular machines,[6] protein polymerization,[7] microtubule buckling,[8] or effects that involve excluded volume or entropic forces such as DNA looping[9] or crowding effects.[10,11] In physics, optical tweezers have various applications from colloidal physics to probing the viscoelastic properties of complex fluids including biological matter.[12−14] Femtonewton or even smaller forces influence phenomena such as thermophoresis,[15] resonances in nanomechanical systems,[16] the Casimir effect,[17,18] or gravitational wave detection.[19] Recent studies reported (sub)femtonewton force measurements in aqueous solutions[9,20−34] (Table S1). For example, Shan et al.[34] measured forces of 0.1 ± 0.6 fN. However, their large uncertainty of ≈0.6 fN underscores the inherent difficulties in achieving precise and reliable measurements at this scale. Attonewton force resolution has only been achieved in vacuum or at cryogenic temperatures but not in biological and soft-matter systems.[16,35] Subfemtonewton force measurements with attonewton resolution under physiological conditions still remain an outstanding challenge. Force measurements are fundamentally limited by Brownian motion. For an overdamped system, the force resolution $\Delta F$ (the thermal noise limit for force) defined as the smallest measurable force during the measurement time $t_{msr}$ is[36]

$$\Delta F = \sqrt{\frac{4k_B T\gamma}{t_{msr}}} \tag{1}$$

where $k_B$ is the Boltzmann constant, $T$ the absolute temperature, and $\gamma$ the drag coefficient of the force probe given by Stokes drag $\gamma = 3\pi\eta d = k_B T/D$ for a sphere with diameter $d$ and diffusion coefficient $D$ suspended in a medium with viscosity $\eta$ far away from a surface.[37] Under physiological conditions, the temperature and viscosity vary little. Thus, the only way to improve the force resolution is to increase the measurement time or decrease the probe size. While eq 1 is

**Received:** May 20, 2025
**Revised:** July 28, 2025
**Accepted:** July 31, 2025
**Published:** August 5, 2025

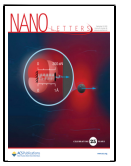





https://doi.org/10.1021/acs.nanolett.5c02698
*Nano Lett.* 2025, 25, 13476−13481

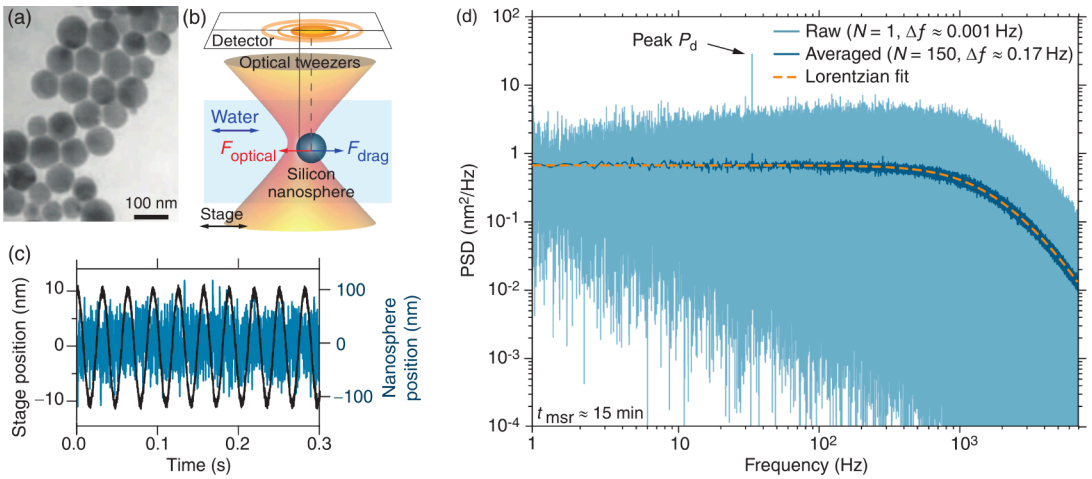


**Figure 1.** Optical tweezers force measurements with silicon nanospheres. (a) Transmission electron microscopy image of silicon nanospheres. (b) A known drag force is applied on a trapped silicon nanosphere by oscillating the aqueous sample relative to the stationary optical trap. The millikelvin precision temperature control was set to 29.500 °C. (c) Nanosphere and stage positions (blue and black line, respectively) as a function of time ($f_d$ = 32 Hz). (d) Power spectral density (PSD) of the data in (c) ($t_{msr} \approx$ 15 min, light blue line with $\Delta f \approx$ 0.001 Hz; dark blue line is the average of 150 PSDs of the same data broken into 150 segments with $\Delta f \approx$ 0.17 Hz, and dashed dark yellow line is a Lorentzian-like fit of the hydrodynamically correct theory[37,44]). Note the oscillation peak at $f_d$ = 32 Hz.

general, our focus is on force measurements with optical tweezers.

Apart from the fundamental limitation of Brownian motion, resolution is limited by instrument noise including thermal drift, optical heating, electronic noise, sound, and mechanical vibrations that affect measurements on different time scales.[4,36,38−42] Thermal drift on long time scales and low-frequency noise eventually limit the measurement time permissible for averaging over Brownian motion and reducing fundamental noise. To overcome challenges of instrument noise and thermal drift, we developed an ultrastable optical tweezers system with temperature feedback control in an isolated environment (Figure 1, section S1 in Supporting Information, and Simmert et al.[43] for a schematic of the used setup).[4,41−43] The setup maintains the sample temperature with millikelvin precision for hours (Figure S1).[41,43] With a well-equilibrated setup, surface drift is minimal with peak-to-peak sample motion of a few nanometers in all dimensions over 1000 s.[4] Thus, our setup ensures stability for long-term measurements and minimizes instrument noise.

To minimize fundamental noise and improve the spatio-temporal and force resolution, according to eq 1, it is advantageous to reduce the probe size as much as possible. However, the trapping efficiency decreases proportional to the probe volume but increases with refractive index mismatch to the medium.[4,45] Thus, nanosphere trapping requires a higher laser power, which can cause heating and low-frequency noise. To mitigate heating, we synthesized nanospheres with a diameter of 81 ± 26 nm (mean ± SD, $N$ = 110) made of crystalline silicon, which has a complex refractive index of $n$ = 3.55 + 0.00009$i$ at our trapping wavelength of 1064 nm[46,47] (Figure 1a, section S2). Thus, unlike metallic nanoparticles, which suffer from plasmonic heating and destabilizing thermal fluctuations,[48] silicon nanospheres have a low absorption and high-refractive index that minimize optical heating and ensure stable trapping conditions with moderate laser powers.[49] When trapping nanospheres a few micrometers away from a glass surface, we expect less than 0.5 K of heating for 100 mW of laser power in our experimental configuration.[50,51] The high-refractive index of silicon nanospheres is also beneficial for detection, as the scattering cross-section is higher compared to silica or polystyrene spheres. Beyond their optical advantages, silicon nanospheres are chemically stable in aqueous solutions for several days.[49] In addition, their surface chemistry allows tunable functionalization with biomolecules, chemical linkers, or coatings, enabling a wide range of applications in biophysics and nanotechnology.

To measure small forces, we trapped silicon nanospheres in deionized water, calibrated the system against thermal and drag forces,[37,44] and asked what the lowest measurable drag force is. Employing back-focal plane interferometry,[37,52,53] we measured the response of the trapped nanosphere to a controlled sinusoidal motion $x(t) = A \sin(2\pi f_d t)$ of the sample chamber driven by a piezo-translation stage, where $x$ is the position, $t$ the time, $A$ the amplitude, and $f_d$ the driving frequency (Figure 1b,c and section S3). The approach is similar to the lock-in technique of Liu et al.[33] that decouples the measurement from low-frequency instrument noise. Using a power spectral density (PSD) analysis, in which the oscillation causes a distinct peak in the one-sided PSD at the stage's driving frequency (Figure 1d, Figure S2), we measured the displacement responsivity $\beta^{-1}$ of the detector (in mV/nm), the trap stiffness $\kappa$ (fN/nm), and the drag coefficient $\gamma$.[37,44] The product $\alpha = \beta\kappa$ is the inverse force responsivity (in fN/mV). To rule out heating effects, we first confirmed that the drag coefficient was within error bars constant when increasing laser power consistent with our expectation of less than 0.5 K heating (Figure S3). For subsequent measurements, we used ≈80 mW in the trapping focus, selected small nanospheres, and confirmed that the measured parameters remained constant (Figure S4). Based on the measured drag coefficient, with the nanospheres relative to their size being far away from any surface,[37,44] and the known temperature and viscosity, the diameter of the trapped nanospheres was 60 ± 3 nm with a trap stiffness of 3.1 ± 0.6 fN/nm (mean ± SD, $N$ = 16, Table S2). Thus, diameters fell within the range measured by transmission electron microscopy (Figure 1a) ruling out that we trapped nanosphere clusters or larger contaminations,


https://doi.org/10.1021/acs.nanolett.5c02698
Nano Lett. 2025, 25, 13476−13481

which are much easier to trap compared with single nanospheres. The consistency also implies that we can calculate the expected thermal noise limit based on the nanosphere diameter.

To test whether we were only limited by thermal and not instrument noise, we measured the force resolution and compared it to the expected thermal noise limit (eq 1, Figure 2, Figure S5). A precise measure for the force resolution is based on the low-frequency limit of the PSD[44]

$$\Delta F_{\mathrm{PSD}} = \alpha\sqrt{P_0 \Delta f} \tag{2}$$

where $P_0 = D_V/(\pi f_c)^2$ is the low-frequency plateau value of a Lorentzian (in $V^2$/Hz), $D_V$ the probe's diffusion coefficient (in $V^2$/s), $f_c = \kappa/(2\pi\gamma)$ the characteristic roll-off frequency, and $\Delta f = 1/t_{\mathrm{msr}}$ the frequency resolution. We determined the force responsivity $\alpha^{-1}$ and $P_0$ by a Lorentzian-like fit of the hydrodynamically correct theory to the PSD.[37,44] Our measurements show that the force resolution was consistent with the thermal noise limit, i.e., $\Delta F_{\mathrm{PSD}} = \Delta F$, and decreased with increased measurement time proportional to $t_{\mathrm{msr}}^{-0.5}$ as expected from eq 1 (Figure 2, Figure S5). The proportionality constant $\alpha\sqrt{P_0}$ (the force sensitivity or smallest detectable force per unit bandwidth) was 2.7 fN $\mathrm{Hz}^{-0.5}$.

For measurement times longer than ≈1000 s, the force resolution was in the attonewton range below 100 aN. For $t_{\mathrm{msr}}$ = 31 min, the force resolution was 63.0 ± 0.1 aN (red solid circle in Figure 2). For a measurement time of 10 s, we had a subfemtonewton force resolution of 0.85 ± 0.02 fN. While our *force sensitivity* was comparable to previous studies, our *force resolution* is about an order of magnitude smaller[33,34] (compare red solid circle with gray triangles in Figure 2, Table S1). Note that it is not advantageous to average PSDs by splitting the data into segments without increasing the measurement time (section S4, Figure S6). An example is shown in Figure 1d, where the peak height at the driving frequency of the averaged PSD becomes comparable to the one of the noise peaks.

What is the lowest drag force that we can directly measure? To test the limits, accuracy, and precision of our system, we reduced the amplitude of the stage oscillation and measured the peak in the PSD and its signal-to-noise ratio (SNR) (Figure 3). With the known oscillation amplitude and drag

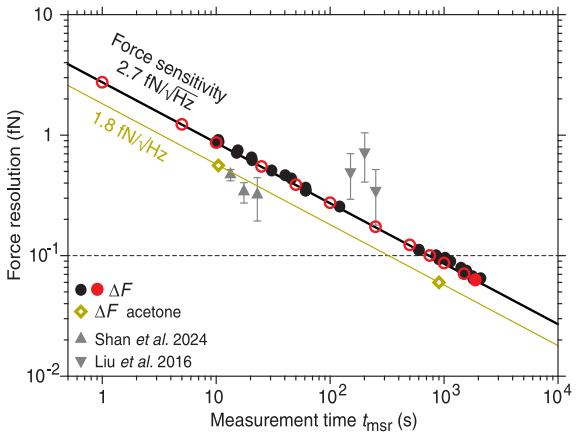


**Figure 2.** Force resolution and sensitivity. Force resolution $\Delta F$ as a function of measurement time $t_{\mathrm{msr}}$. Black solid circles: each data point of $\Delta F_{\mathrm{PSD}}$ (eq 2) corresponds to a different nanosphere and measurement (see Table S2 for the individual measurements). Red solid circle: $\Delta F_{\mathrm{PSD}}$ of the 0.3- fN measurement in Figure 3b. Red open circles: the same nanosphere with different $t_{\mathrm{msr}}$. Dark yellow open diamonds: measurements in acetone. Gray triangles: three smallest values from recent reports.[33,34] The thermal noise limit $\Delta F$ (eq 1) is indicated as solid lines with their slope corresponding to the force sensitivity. The dashed horizontal line corresponds to a 100 aN resolution. Error bars are only shown when larger than the data symbols. For our measurements, relative errors were less than 3%.

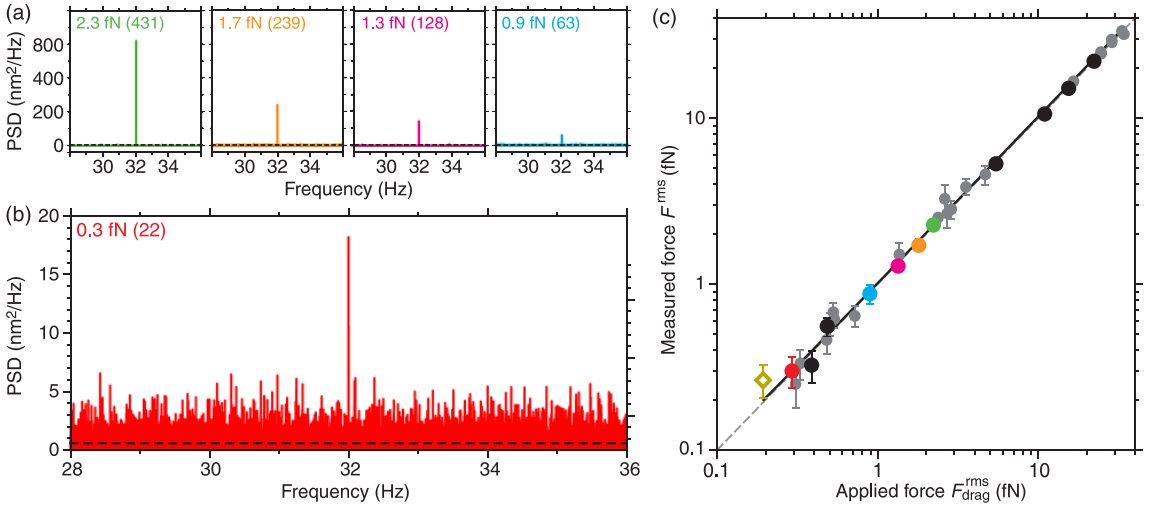


**Figure 3.** Subfemtonewton force measurements. (a) PSDs of a single nanosphere recorded with different oscillation amplitudes ($A$ was 40, 32, 24, and 16 nm from left to right). Forces are indicated with peak-PSD-value SNR in parentheses ($t_{\mathrm{msr}}$ = 10 min, $\Delta f$ = 0.001 67 Hz, black dashed lines are Lorentzian-like fits). (b) Same nanosphere as in (a) with $A$ = 4.6 nm, $t_{\mathrm{msr}}$ = 31 min, and $\Delta f = 5.3 \times 10^{-4}$ Hz. (c) Measured force $F^{\mathrm{rms}}$ vs the applied rms drag force $F_{\mathrm{drag}}^{\mathrm{rms}}$ (eq 3). Colored and black circles are measurements of a single nanosphere with different oscillation amplitudes (colors correspond to (a) and (b), and black circles correspond to measurements with additional oscillation amplitudes). Gray circles: each data point corresponds to a single measurement of different nanospheres trapped with various laser powers on different days. Black line: linear fit with slope 1.03 ± 0.01 and intercept 0.02 ± 0.01. Gray dashed line: $F^{\mathrm{rms}} = F_{\mathrm{drag}}^{\mathrm{rms}}$. Dark yellow open diamond: acetone measurement ($t_{\mathrm{msr}}$ = 15 min). Error bars correspond to the force resolution shown only when larger than the data symbol (see Table S2 for individual values).



https://doi.org/10.1021/acs.nanolett.5c02698
Nano Lett. 2025, 25, 13476−13481

coefficient, we know the applied drag force $F_{drag} = \gamma v$ and can compare it to the measured one based on the oscillation-peak power in the PSD. The directly measured root-mean-square (rms) force derived from the peak PSD value $P_d$ corrected for the thermal background PSD $P_0$ is

$$F^{rms} = \alpha\sqrt{(P_d - P_0)\Delta f} = \pi\gamma A f_d\sqrt{2} = F^{rms}_{drag} \quad (3)$$

where we assumed that $f_d \ll f_c$.[44] For the same nanosphere with stepwise reduced oscillation amplitude, we measured femtonewton forces down to 0.9 ± 0.1 fN ($F^{rms} \pm \Delta F$ with SNR = $F^{rms}/\Delta F$ = 8, Figure 3a). Since the PSD peak power is proportional to the square of the force, even weak forces near the thermal noise limit can be reliably detected in the PSD. For the 0.9 fN peak, its SNR in the PSD was 63. With a longer measurement time, we measured a subfemtonewton force with attonewton resolution of 0.30 ± 0.06 fN (SNR = 4.7, Figure 3b). In a low-viscosity medium such as acetone, we could measure a smaller force of 0.26 ± 0.06 fN (SNR = 4.4) with the same resolution in half the measurement time due to the better force sensitivity of 1.8 fN $Hz^{-0.5}$ (Figure 2, Figure 3c). The directly measured forces $F^{rms}$ corresponded to the applied force as expected from eq 3 ($F^{rms} = F^{rms}_{drag}$) showing that the measurements were not only precise but also accurate (Figure 3c).

Measuring ultraweak forces under biologically relevant conditions remains challenging due to thermal fluctuations and experimental noise. The high-refractive-index silicon nanospheres trapped in ultrastable optical tweezers have an excellent force sensitivity that enables an attonewton force resolution. A further reduction in nanosphere size and SNR will either reduce the measurement time or improve the force resolution in the future. However, measurements in ambient temperature liquids are ultimately limited by eq 1. The large error of 0.6 fN in Shan et al. on a 0.1 fN force corresponds to their force resolution, highlighting the challenges of achieving precise and reliable measurements at the subfemtonewton scale with a good SNR that provides, for example, at least a 95% confidence of the measurement (SNR ≈ 2). Our 0.3 fN measurement with an SNR of 22 for the PSD peak suggests that even weaker forces could be measured under optimized conditions. Our 0.3 fN force was measured with a 3 fN/nm trap stiffness and corresponds to detecting a 1 Å rms displacement in a 220 nm peak-to-peak (6 SD) background of Brownian motion illustrating that molecular scale displacements and subfemtonewton forces can be measured under the noisy conditions in ambient liquids.

Using, for example, click chemistry[54] or lipid bilayer coatings,[4] we expect that silicon nanospheres can be functionalized with biomolecules, such as DNA or motor proteins. Optical trapping experiments using germanium nanospheres have shown that laser powers up to 500 mW do not cause photodamage on biomolecules.[4] As silicon absorbs much less compared to germanium at 1064 nm, less heating is expected, which may allow even higher trapping powers. Alternatively, larger spheres up to a diameter of about 260 nm are expected to be trappable[55] that would need less power to achieve the same trap stiffness at the price of a lower resolution. Compared with germanium, silicon nanospheres are more robust to synthesize and stable in aqueous solutions. Thus, they are promising probes for applications in biophysics and nanotechnology that require high spatiotemporal and/or force resolution. While nanosphere diameters can be reduced further, limits in trapping power of conventional optical tweezers with respect to trap stiffness and maximum forces will quickly be reached because of the cubic dependence on the probe size. For example, reducing the diameter by a factor of 2, in our case to a diameter of 30 nm, would require 8 times more laser power to achieve the same trap stiffness. Using less power weakens the trap and increases the probability that particles escape the trap due to Brownian motion. For our nanospheres, we required about 25 mW for stable trapping over minutes to hours consistent with calculations.[55] Plasmonic tweezers are promising to push the spatiotemporal and force limits further as they can trap single proteins without the need of a nanosphere handle at comparable laser powers to the ones used here.[56,57] However, apart from limitations on the experimental geometry for biophysical measurements, quantification of displacements and forces, while accounting for heating effects, is still challenging in plasmonic tweezers.[57]

Our advancements exceed prior benchmarks for weak force detection (Table S1), opening new possibilities for studying nanoscale interactions with unparalleled precision. This ability has implications in biophysics, nanotechnology, and fundamental physics. Our findings lay the foundation for discoveries in force spectroscopy and related fields.

## ■ ASSOCIATED CONTENT

### Supporting Information

The Supporting Information is available free of charge at https://pubs.acs.org/doi/10.1021/acs.nanolett.5c02698.

Section S1 on setup and data acquisition; section S2 on silicon nanosphere synthesis and sample preparation; section S3 on experimental conditions and data analysis; section S4 on force resolution and averaging of PSDs; Figures S1−S6; Tables S1 and S2 (PDF)

## ■ AUTHOR INFORMATION


### Corresponding Authors

**Anita Jannasch** − *Center for Plant Molecular Biology (ZMBP), Eberhard Karls Universität Tübingen, 72076 Tübingen, Germany;* orcid.org/0000-0002-5845-7869; Email: anita.jannasch@uni.tuebingen.de

**Erik Schäffer** − *Center for Plant Molecular Biology (ZMBP), Eberhard Karls Universität Tübingen, 72076 Tübingen, Germany;* orcid.org/0000-0001-7876-085X; Email: erik.schaeffer@uni.tuebingen.de

### Authors

**Aleksandr Kostarev** − *Center for Plant Molecular Biology (ZMBP), Eberhard Karls Universität Tübingen, 72076 Tübingen, Germany;* orcid.org/0000-0002-9955-1069

**Mohammad K. Abdosamadi** − *Center for Plant Molecular Biology (ZMBP), Eberhard Karls Universität Tübingen, 72076 Tübingen, Germany*

**Hiroshi Sugimoto** − *Graduate School of Engineering, Kobe University, Kobe 657-8501, Japan;* orcid.org/0000-0002-1520-0940

**Minoru Fujii** − *Graduate School of Engineering, Kobe University, Kobe 657-8501, Japan;* orcid.org/0000-0003-4869-7399

Complete contact information is available at: https://pubs.acs.org/10.1021/acs.nanolett.5c02698




https://doi.org/10.1021/acs.nanolett.5c02698
Nano Lett. 2025, 25, 13476−13481

### Author Contributions

[¶]A.K. and M.K.A. contributed equally. E.S. designed the research. A.K. performed all measurements. M.K.A. performed preliminary experiments and optimized the experimental procedures. A.K. and A.J. analyzed the data. H.S. and M.F. synthesized the silicon nanospheres. A.K., A.J., and E.S. wrote the manuscript.

### Notes

The authors declare no competing financial interest.

## ■ ACKNOWLEDGMENTS

The authors thank Rahul Vaippully and Shu Yao Leong for comments on the manuscript. This work was supported by the Deutsche Forschungsgemeinschaft (DFG, CRC 1101, Project A04), the University of Tübingen, the JST FOREST Program (Grant JPMJFR213L), and the Kobe University Strategic International Collaborative Research Grant.

## ■ REFERENCES

(1) Block, S. M.; Goldstein, L. S. B.; Schnapp, B. J. Bead movement by single kinesin molecules studied with optical tweezers. *Nature* **1990**, *348*, 348−352.
(2) Mehta, A. D.; Rief, M.; Spudich, J. A.; Smith, D. A.; Simmons, R. M. Single-molecule biomechanics with optical methods. *Science* **1999**, *283*, 1689−1695.
(3) Bustamante, C. J.; Chemla, Y. R.; Liu, S.; Wang, M. D. Optical tweezers in single-molecule biophysics. *Nat. Rev. Methods Primers* **2021**, *1*, 25.
(4) Sudhakar, S.; Abdosamadi, M. K.; Jachowski, T. J.; Bugiel, M.; Jannasch, A.; Schäffer, E. Germanium nanospheres for ultraresolution picotensiometry of kinesin motors. *Science* **2021**, *371*, No. eabd9944.
(5) Ma, X.; Jannasch, A.; Albrecht, U.-R.; Hahn, K.; Miguel-López, A.; Schäffer, E.; Sánchez, S. Enzyme-powered hollow mesoporous Janus nanomotors. *Nano Lett.* **2015**, *15*, 7043−7050.
(6) Chugh, M.; Reißner, M.; Bugiel, M.; Lipka, E.; Herrmann, A.; Roy, B.; Müller, S.; Schäffer, E. Phragmoplast orienting kinesin 2 is a weak motor switching between processive and diffusive modes. *Biophys. J.* **2018**, *115*, 375−385.
(7) Herling, T. W.; Garcia, G. A.; Michaels, T. C. T.; Grentz, W.; Dean, J.; Shimanovich, U.; Gang, H.; Müller, T.; Kav, B.; Terentjev, E. M.; Dobson, C. M.; Knowles, T. P. J. Force generation by the growth of amyloid aggregates. *Proc. Natl. Acad. Sci. U.S.A.* **2015**, *112*, 9524−9529.
(8) Kikumoto, M.; Kurachi, M.; Tosa, V.; Tashiro, H. Flexural rigidity of individual microtubules measured by a buckling force with optical traps. *Biophys. J.* **2006**, *90*, 1687−1696.
(9) Chen, Y.-F.; Milstein, J. N.; Meiners, J.-C. Femtonewton entropic forces can control the formation of protein-mediated DNA loops. *Phys. Rev. Lett.* **2010**, *104*, 048301.
(10) Sozanski, K.; Ruhnow, F.; Wiśniewska, A.; Tabaka, M.; Diez, S.; Hołyst, R. Small crowders slow down kinesin-1 stepping by hindering motor domain diffusion. *Phys. Rev. Lett.* **2015**, *115*, 218102.
(11) Nettesheim, G.; Nabti, I.; Murade, C. U.; Jaffe, G. R.; King, S. J.; Shubeita, G. T. Macromolecular crowding acts as a physical regulator of intracellular transport. *Nat. Phys.* **2020**, *16*, 1144−1151.
(12) Robertson-Anderson, R. M. Optical tweezers microrheology: from the basics to advanced techniques and applications. *ACS Macro Lett.* **2018**, *7*, 968−975.
(13) Bevan, M. A.; Eichmann, S. L. Optical microscopy measurements of kT-scale colloidal interactions. *Curr. Opin. Colloid Interface Sci.* **2011**, *16*, 149−157.
(14) Català-Castro, F.; Schäffer, E.; Krieg, M. Exploring cell and tissue mechanics with optical tweezers. *J. Cell Sci.* **2022**, *135*, jcs259355.
(15) Helden, L.; Eichhorn, R.; Bechinger, C. Direct measurement of thermophoretic forces. *Soft Matter* **2015**, *11*, 2379−2386.
(16) Zhang, Z.; Xu, N.; Huang, Z.; Lai, J.; Liu, J.; Deng, G.; Wang, X.; Zhao, W. High-sensitivity force sensors based on novel materials. *Adv. Devices Instrum.* **2023**, *4*, 0019.
(17) Chen, F.; Mohideen, U.; Klimchitskaya, G. L.; Mostepanenko, V. M. Demonstration of the lateral Casimir force. *Phys. Rev. Lett.* **2002**, *88*, 101801.
(18) Ether, D. S., Jr.; Pires, L. B.; Umrath, S.; Martinez, D.; Ayala, Y.; Pontes, B.; de S. Araujo, G. R.; Frases, S.; Ingold, G.-L.; Rosa, F. S. S.; et al. Probing the Casimir force with optical tweezers. *EPL* **2015**, *112*, 44001.
(19) Arvanitaki, A.; Geraci, A. A. Detecting high-frequency gravitational waves with optically levitated sensors. *Phys. Rev. Lett.* **2013**, *110*, 071105.
(20) Pollard, M. R.; Botchway, S. W.; Chichkov, B.; Freeman, E.; Halsall, R. N. J.; Jenkins, D. W. K.; Loader, I.; Ovsianikov, A.; Parker, A. W.; Stevens, R.; Turchetta, R.; Ward, A. D.; Towrie, M. Optically trapped probes with nanometer-scale tips for femto-Newton force measurement. *New J. Phys.* **2010**, *12*, 113056.
(21) Fontes, A.; Giorgio, S.; de Castro, A. B., Jr.; Neto, V. M.; de Y. Pozzo, L.; Marques, G. P.; Barbosa, L. C.; Cesar, C. L. Determination of femto Newton forces and fluid viscosity using optical tweezers: application to Leishmania amazonensis. *Proc. SPIE* **2005**, *5699*, 419−425.
(22) Hohng, S.; Zhou, R.; Nahas, M. K.; Yu, J.; Schulten, K.; Lilley, D. M. J.; Ha, T. Fluorescence-force spectroscopy maps two-dimensional reaction landscape of the Holliday junction. *Science* **2007**, *318*, 279−283.
(23) Rohrbach, A. Switching and measuring a force of 25 femtoNewtons with an optical trap. *Opt. Express* **2005**, *13*, 9695−9701.
(24) Imasato, H.; Yamakawa, T. Measurement of dielectrophoretic force by employing controllable gravitational force. *J. Electrophor.* **2008**, *52*, 1−8.
(25) Neuman, K. C.; Nagy, A. Single-molecule force spectroscopy: optical tweezers, magnetic tweezers and atomic force microscopy. *Nat. Methods* **2008**, *5*, 491−505.
(26) Gibson, G. M.; Leach, J.; Keen, S.; Wright, A. J.; Padgett, M. J. Measuring the accuracy of particle position and force in optical tweezers using high-speed video microscopy. *Opt. Express* **2008**, *16*, 14561−14570.
(27) Rudhardt, D.; Bechinger, C.; Leiderer, P. Repulsive depletion interactions in colloid-polymer mixtures. *J. Phys.: Condens. Matter* **1999**, *11*, 10073.
(28) Stoev, I. D.; Seelbinder, B.; Erben, E.; Maghelli, N.; Kreysing, M. Highly sensitive force measurements in an optically generated, harmonic hydrodynamic trap. *eLight* **2021**, *1*, 7.
(29) Prieve, D. C. Measurement of colloidal forces with TIRM. *Adv. Colloid Interface Sci.* **1999**, *82*, 93−125.
(30) Maragò, O. M.; Jones, P. H.; Bonaccorso, F.; Scardaci, V.; Gucciardi, P. G.; Rozhin, A. G.; Ferrari, A. C. Femtonewton force sensing with optically trapped nanotubes. *Nano Lett.* **2008**, *8*, 3211−3216.
(31) Sainis, S. K.; Germain, V.; Mejean, C. O.; Dufresne, E. R. Electrostatic interactions of colloidal particles in nonpolar solvents: role of surface chemistry and charge control agents. *Langmuir* **2008**, *24*, 1160.
(32) Zensen, C.; Villadsen, N.; Winterer, F.; Keiding, S. R.; Lohmüller, T. Pushing nanoparticles with light — A femtonewton resolved measurement of optical scattering forces. *APL Photonics* **2016**, *1*, 026102.
(33) Liu, L.; Kheifets, S.; Ginis, V.; Capasso, F. Subfemtonewton force spectroscopy at the thermal limit in liquids. *Phys. Rev. Lett.* **2016**, *116*, 228001.
(34) Shan, X.; Ding, L.; Wang, D.; Wen, S.; Shi, J.; Chen, C.; et al. Sub-femtonewton force sensing in solution by super-resolved photonic force microscopy. *Nat. Photonics* **2024**, *18*, 913.
(35) Ranjit, G.; Atherton, D. P.; Stutz, J. H.; Cunningham, M.; Geraci, A. A. Attonewton force detection using microspheres in a dual-beam optical trap in high vacuum. *Phys. Rev. A* **2015**, *91*, 051805.


https://doi.org/10.1021/acs.nanolett.5c02698
*Nano Lett.* 2025, 25, 13476−13481

(36) Gittes, F.; Schnurr, B.; Olmsted, P. D.; MacKintosh, F. C.; Schmidt, C. F. Microscopic viscoelasticity: shear moduli of soft materials determined from thermal fluctuations. *Phys. Rev. Lett.* **1997**, *79*, 3286−3289.
(37) Schäffer, E.; Nørrelykke, S. F.; Howard, J. Surface forces and drag coefficients of microspheres near a plane surface measured with optical tweezers. *Langmuir* **2007**, *23*, 3654−3665.
(38) Smith, S. B.; Cui, Y.; Bustamante, C. *Biophotonics, Part B*; Methods in Enzymology; Academic Press, 2003; Vol. *361*; pp 134−162.
(39) Czerwinski, F.; Richardson, A. C.; Oddershede, L. B. Quantifying noise in optical tweezers by Allan variance. *Opt. Express* **2009**, *17*, 13255−13269.
(40) Carter, A. R.; Seol, Y.; Perkins, T. T. Precision surface-coupled optical-trapping assay with one-basepair resolution. *Biophys. J.* **2009**, *96*, 2926−2934.
(41) Mahamdeh, M.; Schäffer, E. Optical tweezers with millikelvin precision of temperature-controlled objectives and base-pair resolution. *Opt. Express* **2009**, *17*, 17190−17199.
(42) Hermsdorf, G. L.; Szilagyi, S. A.; Rösch, S.; Schäffer, E. High performance passive vibration isolation system for optical tables using six-degree-of-freedom viscous damping combined with steel springs. *Rev. Sci. Instrum.* **2019**, *90*, 015113.
(43) Simmert, S.; Abdosamadi, M. K.; Hermsdorf, G.; Schäffer, E. LED-based interference-reflection microscopy combined with optical tweezers for quantitative three-dimensional microtubule imaging. *Opt. Express* **2018**, *26*, 14499−14513.
(44) Tolić-Nørrelykke, S. F.; Schäffer, E.; Howard, J.; Pavone, F. S.; Jülicher, F.; Flyvbjerg, H. Calibration of optical tweezers with positional detection in the back focal plane. *Rev. Sci. Instrum.* **2006**, *77*, 103101.
(45) Bormuth, V.; Jannasch, A.; Ander, M.; van Kats, C. M.; van Blaaderen, A.; Howard, J.; Schäffer, E. Optical trapping of coated microspheres. *Opt. Express* **2008**, *16*, 13831−13844.
(46) Sugimoto, H.; Okazaki, T.; Fujii, M. Mie resonator color inks of monodispersed and perfectly spherical crystalline dilicon nanoparticles. *Adv. Opt. Mater.* **2020**, *8*, 2000033.
(47) Polyanskiy, M. N. Refractiveindex.info database of optical Constants. *Sci. Data* **2024**, *11*, 94.
(48) Seol, Y.; Carpenter, A. E.; Perkins, T. T. Gold nanoparticles: enhanced optical trapping and sensitivity coupled with significant heating. *Opt. Lett.* **2006**, *31*, 2429−2431.
(49) Hinamoto, T.; Hotta, S.; Sugimoto, H.; Fujii, M. Colloidal solutions of silicon nanospheres toward all-dielectric optical metafluids. *Nano Lett.* **2020**, *20*, 7737−7743.
(50) Peterman, E. J. G.; Gittes, F.; Schmidt, C. F. Laser-induced heating in optical traps. *Biophys. J.* **2003**, *84*, 1308−1316.
(51) Jannasch, A.; Mahamdeh, M.; Schäffer, E. Inertial effects of a small Brownian particle cause a colored power spectral density of thermal noise. *Phys. Rev. Lett.* **2011**, *107*, 228301.
(52) Allersma, M. W.; Gittes, F.; deCastro, M. J.; Stewart, R. J.; Schmidt, C. F. Two-dimensional tracking of ncd motility by back focal plane interferometry. *Biophys. J.* **1998**, *74*, 1074−85.
(53) Pralle, A.; Prummer, M.; Florin, E.-L.; Stelzer, E.; Hörber, J. Three-dimensional high-resolution particle tracking for optical tweezers by forward scattered light. *J. Microsc.* **1999**, *44*, 378−386.
(54) Siegel, N.; Hasebe, H.; Chiarelli, G.; Garoli, D.; Sugimoto, H.; Fujii, M.; Acuna, G. P.; Kołątaj, K. Universal click-chemistry approach for the DNA functionalization of nanoparticles. *J. Am. Chem. Soc.* **2024**, *146*, 17250−17260.
(55) Länk, N. O.; Johansson, P.; Käll, M. Directional scattering and multipolar contributions to optical forces on silicon nanoparticles in focused laser beams. *Opt. Express* **2018**, *26*, 29074−29085.
(56) Pang, Y.; Gordon, R. Optical trapping of a single protein. *Nano Lett.* **2012**, *12*, 402−406.
(57) Zhang, Y.; Min, C.; Dou, X.; Wang, X.; Urbach, H. P.; Somekh, M. G.; Yuan, X. Plasmonic tweezers: for nanoscale optical trapping and beyond. *Light Sci. Appl.* **2021**, *10*, 59.



https://doi.org/10.1021/acs.nanolett.5c02698
*Nano Lett.* 2025, 25, 13476−13481

# SUPPORTING INFORMATION

# Attonewton force resolution measurements with silicon nanospheres at the thermal noise limit in ambient-temperature liquids

Aleksandr Kostarev,[†,¶] Mohammad K. Abdosamadi,[†,¶] Hiroshi Sugimoto,[‡] Minoru Fujii,[‡] Anita Jannasch,[*,†] and Erik Schäffer[*,†]

†*Center for Plant Molecular Biology (ZMBP), Eberhard Karls Universität Tübingen, 72076 Tübingen, Germany*

‡*Graduate School of Engineering, Kobe University, Kobe, 657-8501, Japan*

¶*These authors contributed equally*

E-mail: anita.jannasch@uni.tuebingen.de; erik.schaeffer@uni.tuebingen.de

## Table of Contents

# Supporting text

## S1 Setup & data acquisition

Measurements were performed in a custom-built, single-beam optical tweezers setup described in detail here.[1] Briefly, the optical tweezers are combined with interference reflection microscopy[1,2] (IRM) that provides sufficient contrast to image single nanospheres.[3] To ensure high stability, the temperature was controlled using a feedback system with millikelvin precision, set to 29.500 °C (Fig. S1).[1,4] The temperature control system enables measurements at temperatures up to 37 °C.[4] The setup is mounted on an active vibration isolation table[1] and enclosed in a custom-built chamber.[5] The nanospheres were trapped using a 1064-nm laser. The power spectral density (PSD) of the trapped nanosphere motion was computed from time traces[6] recorded from a quadrant photo diode (QP45-Q HVSD, First Sensor AG, Germany) by back-focal-plane interferometry with a sampling rate of 25600 $s^{-1}$. The piezo-translation stage (LFHS3, Piezoconcept, Bron, France, updated since[1]) was oscillated at 32 Hz with various, sub-nanometer-precision amplitudes to apply a controlled drag force on the nanospheres. Stage displacements were measured and recorded from the stage's sensor output simultaneously with the photo diode signals.

## S2 Silicon nanosphere synthesis & sample preparation

Silicon nanospheres were synthesized via high-temperature annealing of silicon monoxide, followed by hydrofluoric acid etching and dispersion in solvent described in detail here.[7,8] The diameter measured by transmission electron microscopy was $81 \pm 26$ nm (Mean $\pm$ SD, $N = 110$, inset Fig. 1a). The nanospheres were produced as powder and were dissolved in pure 99.8% absolute ethanol for storage. Before the experiment, the nanospheres were diluted in purified Type 1 water (18.2 MΩ cm, Nanopure System MilliQ reference with a Q-POD and Biopak filter) and sonicated on a table sonicator for 2 minutes. Then the diluted

sample was introduced into a custom flow cell assembled from coverslips. Coverslips were cleaned once with the detergent Mucasol and twice with anhydrous ethanol. Two Parafilm M stripes were sandwiched between the bottom (22×22 mm, #1 1/2, Corning 2850-22) and top coverslip (18×18 mm, #0, Menzel-Gläser) forming 1–2-mm wide and ≈100-µm high channel between them. The flow cell was briefly heated to 140 °C to melt the Parafilm layer and form a stable channel. After addition of the sample solution in the channel, its openings were sealed with nail polish to prevent evaporation-induced flows. Afterwards the sample flow cell was mounted in the optical tweezers setup for at least one hour prior to measurements to ensure stable thermal conditions. Since the diameter affects resolution, we aimed to trap the smallest nanospheres visible in IRM, resulting in an average diameter of $60 \pm 3$ nm for the analyzed, trapped nanospheres.

## S3 Experimental conditions & data analysis

To minimize surface effects of the drag coefficient,[9] nanospheres were trapped and measured more than 4 µm away from the surface. To quantify low-frequency instrument noise and verify that the observed peak at 32 Hz was due to our applied drag force and not caused by laser fluctuations, electronic noise or other influences, we measured the detector signal without a trapped nanosphere (Fig. S2). Only low-frequency noise ($< 1$ Hz) and peaks at high frequencies ($> 7$ kHz) in the PSD of the nanosphere originated from instrument noise. At the stage driving frequency of 32 Hz, instrument noise was more than two orders of magnitude below the measurement signal. The drag coefficient did not depend on trapping power confirming that no significant amount of heating due to absorption of the silicon nanosphere or the surrounding water was present (Fig. S3). Increased temperatures would decrease the viscosity and drag coefficient. Measurements in Fig. 2 (red circles) and Fig. 3 (colored circles) are based on data recorded with a single nanosphere continuously trapped over 2 h with 80 mW trapping power in the laser focus. Between drag force measurements,

several calibration measurements were performed with a 615 nm oscillation amplitude, a 4 Hz frequency resolution, and averaging of 40 PSDs.[6] During the 2 h-measurement, the drag coefficient ($0.45 \pm 0.01$ nNs/m), trap stiffness ($3.1 \pm 0.1$ fN/nm), inverse displacement responsivity ($27.1 \pm 0.7$ nm/mV), and inverse force responsivity ($84.2 \pm 0.7$ fN/mV), remained constant (Fig. S4). For each individual nanosphere, the uncertainties in diameter and trap stiffness were less than 5 % based on fitting errors. These calibration controls show that the setup was stable and confirmed that no additional nanosphere or contamination was trapped (Table S2).

## S4 Force resolution & averaging of PSDs

Instead of using the low-frequency limit of the PSD to calculate the force resolution (Eq. 2), an alternative approach is based on the standard deviation (SD) of the individual power-spectral values $P(f)$ at a certain frequency $f$. Each value $P(f)$ is exponentially distributed with its standard deviation $\sigma\,[P(f)]$ being equal to its mean value.[10,11] Therefore, we can also determine the force resolution based on the noise in the plateau region (assuming that $f_d \ll f_c$)

$$\Delta F_{\mathrm{SD}} = \alpha \sqrt{\sigma\left[P(f \mid f_d - \tfrac{1}{2} f_b \leq f \leq f_d + \tfrac{1}{2} f_b)\right] \Delta f}, \tag{S1}$$

where $\sigma[\ldots]$ denotes the standard deviation and $f_b$ is the bandwidth over which the standard deviation is calculated. We used $f_b = 40$ Hz and excluded the peak at $f_d$. Our measurements show that the estimator for the force resolution $\Delta F_{\mathrm{PSD}}$ was more precise compared to $\Delta F_{\mathrm{SD}}$ but both estimates were consistent with the thermal noise limit (Fig. S5) and deviated less than 6 % from it.

Since the signal-to-noise ratio (SNR) of individual PSD values $P(f)$ is one, averaging over $N$ power spectra reduces noise on the individual PSD values $P(f)$.[6,10,11] Averaging of PSDs implies that the total measurement time $t_{\mathrm{msr}}$ is divided into $N$ segments each of duration $t_{\mathrm{msr}}/N$. Thus, the frequency resolution for an individual PSD gets worse with $N$ according

to $\Delta f = N/t_{\mathrm{msr}}$. The force resolution estimate of $\Delta F_{\mathrm{PSD}}$ (Eq. 2) scales with the square root of the average power $P_0\Delta f$ of the Lorentzian plateau value in the low-frequency limit. Since we account for the small bias of the fit value $P_0$ on $N$ during the fitting procedure,[11,12] its mean fit value does not depend on $N$. Thus, because the frequency resolution increases proportional to $N$, $\Delta F_{\mathrm{PSD}}$ increases with the square-root of $N$, $\Delta F_{\mathrm{PSD}} = \Delta F_1\sqrt{N}$, where $\Delta F_1$ is the force resolution for a non-averaged, single PSD. Since our applied drag force does not depend on whether we average PSDs, the power in the peak at our driving frequency $P_d\Delta f$ is constant and independent of $N$, while $\Delta f$ increases linearly with $N$. Therefore, the height of the peak $P_d$ decreases with the inverse of $N$, $P_d \propto 1/N$ that the power in the peak remains constant. Because averaging decreases the peak height, it will disappear in the noise upon averaging, which can be seen in Fig. 1d for the averaged PSD data. The SNR of the peak height will decrease accordingly.

Interestingly, our other estimate for the force resolution $\Delta F_{\mathrm{SD}}$ (Eq. S1) scales differently with $N$. By averaging PSDs, the standard deviation of the individual PSD values reduces with the square root of $N$, $\sigma[P(f)]/\sqrt{N}$. Thus, the force resolution scales with $N$ as

$$\Delta F_{\mathrm{SD}} \propto \sqrt{\frac{\sigma\left[P(f)\right]}{\sqrt{N}}\frac{N}{t_{\mathrm{msr}}}} \propto \sqrt[4]{N}. \tag{S2}$$

We determined both force resolution estimators for an increasing number of averaged PSDs (Fig. S6). Both estimators scaled and increased as expected with $N$. Thus, the best force resolution is achieved without averaging for a single PSD that has the best frequency resolution. Another way of thinking about it is, that the least amount of Brownian noise is contained in the smallest bandwidth of the best frequency resolution.

# Supporting figures

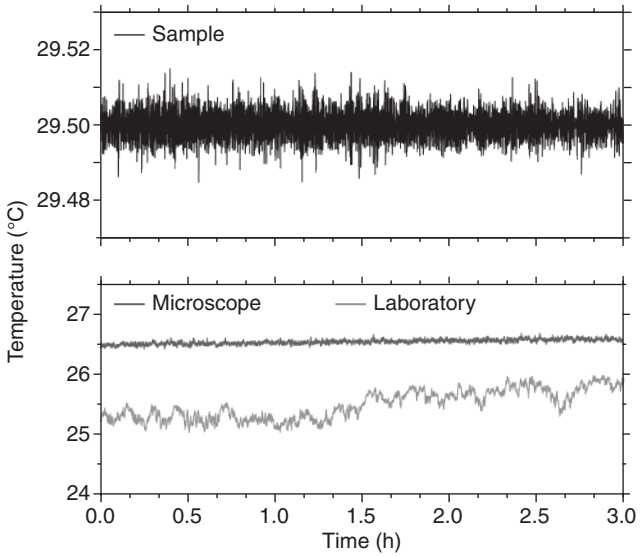


Figure S1: Temperature during the experiment of the sample (measured at the top of the oil-immersion objective,[4] top, black, $29.500 \pm 0.003\,^{\circ}\mathrm{C}$ [mean $\pm$ SD]), the custom-built microscope body inside the setup chamber (bottom, dark grey, $26.56 \pm 0.04\,^{\circ}\mathrm{C}$), and the outside laboratory room (bottom, light grey, $25.53 \pm 0.25\,^{\circ}\mathrm{C}$), indicating stable conditions throughout.

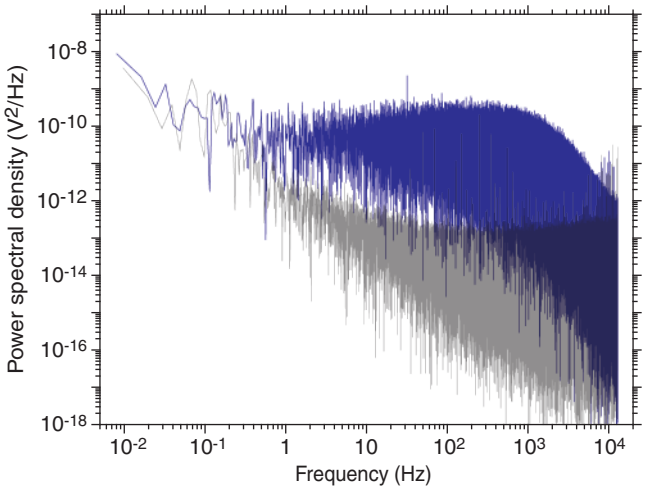


Figure S2: PSD of a trapped silicon nanosphere (blue) and the laser signal without a trapped nanosphere but with the same power (grey, half-transparent). The data from the nanosphere is the same as in Fig. 1d but not calibrated and plotted with an extended frequency range.

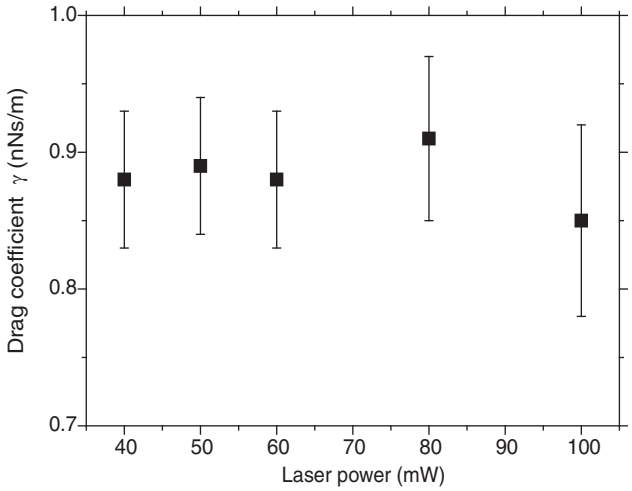


Figure S3: Measured drag coefficient $\gamma$ of a single, trapped silicon nanosphere with diameter $d = 77 \pm 3\,\mathrm{nm}$ as a function of the laser power in the trapping focus. For each calibration measurement, we averaged 40 PSDs with $\Delta f = 8\,\mathrm{Hz}$, $A = 615\,\mathrm{nm}$, and $f_d = 32\,\mathrm{Hz}$.

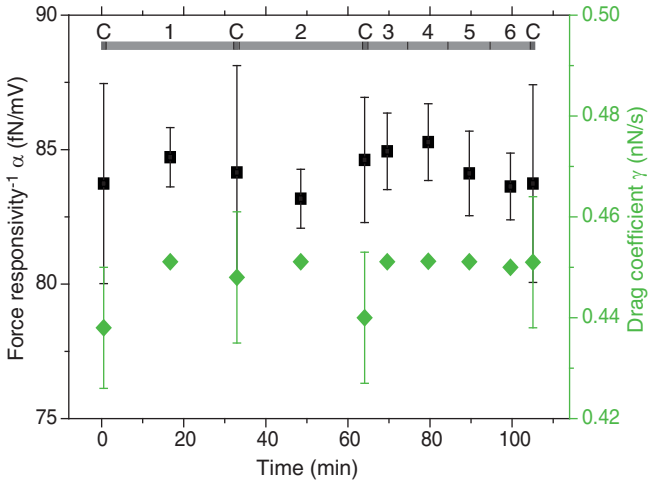


Figure S4: Inverse force responsivity $\alpha$ (black squares, left vertical axis) and drag coefficient $\gamma$ (green diamonds, right vertical axis) for single nanosphere measurements shown in Fig. 3a,b. The nanosphere remained trapped for 2 h during repeated measurements. The gray bar at the top with dark gray markings indicates the measurement duration ($t_{\mathrm{msr}}$) for each data point (measurement 1–6). Between drag force measurements, several calibration (C) measurements were performed.

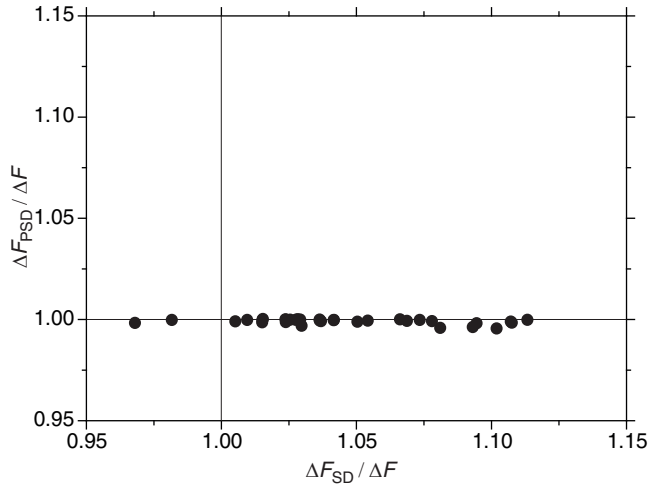


Figure S5: Force resolution $\Delta F_{\mathrm{PSD}}$ (Eq. 2) plotted versus $\Delta F_{\mathrm{SD}}$ (Eq. S1) both normalized by the thermal noise limit $\Delta F$ (Eq. 1). $\Delta F_{\mathrm{PSD}}$ was more precise than $\Delta F_{\mathrm{SD}}$ but both estimates were consistent with the thermal noise limit. Data are from 16 different nanospheres with different measurement times.

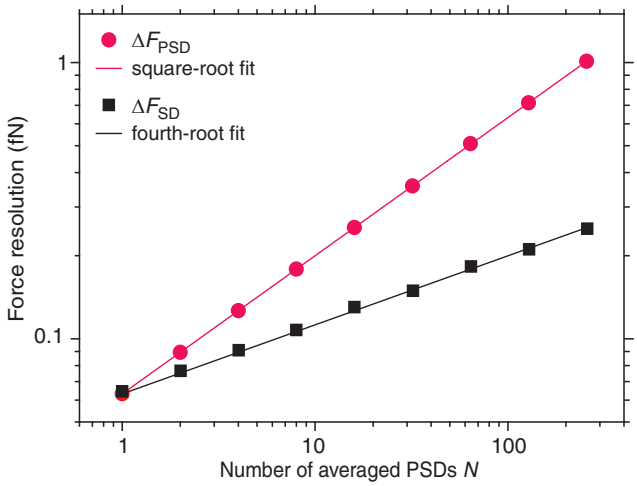


Figure S6: Force resolution $\Delta F_{\mathrm{PSD}}$ (red circles) and force resolution $\Delta F_{\mathrm{SD}}$ (black squares) as a function of the number of averaged PSDs $N$ fitted to power laws (see Sect. S4 for details). Data corresponds to the 0.3-fN measurement shown in Fig. 3b. The red and black line are fits of $\Delta F = \Delta F_1 N^p$ with the exponent $p$ equal to $\frac{1}{2}$ and $\frac{1}{4}$, respectively. Both fits resulted in the same force resolution for a single PSD of $\Delta F_1 = 63\,\mathrm{aN}$, corresponding to the thermal noise limit and force resolution of the non-averaged PSD.

# Supporting tables

Table S1: Sub-piconewton force measurements. Displayed are the smallest measured force ($F$), force resolution ($\Delta F$), force sensitivity ($S_F^{1/2}$), and type of the applied force (origin of the force) for exemplary publications.

| $F$ (fN) | $\Delta F$ (fN) | $S_F^{1/2}$ (fN/Hz$^{0.5}$) | Origin of the force | Reference |
|---|---|---|---|---|
| 240 | | ≈24 | Optical pressure | Pollard 2010[13] |
| 200 | | | Optical pressure | Fontes 2005[14] |
| ≈100 | | | Optical pressure | Hohng 2007[15] |
| 25.6 | 2.2 fN | | Optical pressure | Rohrbach 2005[16] |
| 25 | | | Dielectrophoresis | Imasato 2008[17] |
| 20 | | | Thermophoretic motion | Helden 2015[18] |
| | 10 | | Thermal motion | Gibson 2008[19] |
| 45 | 10 | | Depletion force | Rudhardt 1999[20] |
| 8-12 | | | Magnetic force | Stoev 2021[21] |
| 10 | | | Depletion force | Prieve 1999[22] |
| | ≈8 | | Optical pressure | Marago 2008[23] |
| ≈8 | ≈1.8 | | Thermally activated state transition | Chen 2012[24] |
| | ≈5 | | Surface electrical charges | Sainis 2008[25] |
| | 2.2 | | Optical pressure | Zensen 2016[26] |
| 10 | <1 fN | | Optical pressure | Liu 2016[27] |
| 0.1 | 0.6 | 1.6 | Electrophoresis forces | Shan 2024[28] |
| **0.3** | **0.06** | **2.7** | **Drag force** | **Our measurement** |

Table S2: Parameter values of the data plotted in Fig. 2 and Fig. 3. Listed are the measured force ($F^{\mathrm{rms}}$), applied drag force ($F_{\mathrm{drag}}$), force resolution ($\Delta F_{\mathrm{PSD}}$ and $\Delta F_{\mathrm{SD}}$), signal-to-noise ratio for the PSD peak ($\mathrm{SNR}_{\mathrm{PSD}}$) and for force ($\mathrm{SNR}_F$), fitted zero-frequency limit of Lorentzian plateau value ($P_0$), amplitude of oscillation ($A$), frequency resolution ($\Delta f$), trap stiffness ($\kappa$), detector displacement responsivity ($\beta^{-1}$, different neutral density filters in front of the QPD detector led to different magnitudes of values), measured nanosphere diameter ($d$), and measurement time ($t_{\mathrm{msr}}$). The last two rows correspond to the measurements in acetone. The maximum coefficient of variation for $\kappa$ and $\beta$ did not exceed 1%.

| $F^{\mathrm{rms}}$ (fN) | $F^{\mathrm{rms}}_{\mathrm{drag}}$ (fN) | $\Delta F_{\mathrm{PSD}}$ (fN) | $\Delta F_{\mathrm{SD}}$ (fN) | $\mathrm{SNR}_{\mathrm{PSD}}$ | $\mathrm{SNR}_F$ | $P_0$ ($\mathrm{nm}^2$/Hz) | $A$ (nm) | $\Delta f$ (Hz) | $\kappa$ (fN/nm) | $\beta$ (nm/mV) | $d$ (nm) | $t_{\mathrm{msr}}$ (s) |
|---|---|---|---|---|---|---|---|---|---|---|---|---|
| 0.30 | 0.29 | 0.063 | 0.065 | 22.4 | 4.7 | 0.76 | 4.6 | 0.00053 | 3.15 | 26.9 | 59.3 | 1886.8 |
| 0.32 | 0.39 | 0.073 | 0.076 | 19.9 | 4.5 | 0.74 | 5.7 | 0.00067 | 3.28 | 25.1 | 62.7 | 1500.8 |
| 0.56 | 0.49 | 0.065 | 0.066 | 75.0 | 8.7 | 0.76 | 7.6 | 0.00055 | 3.15 | 26.4 | 59.3 | 1808.0 |
| 0.88 | 0.89 | 0.112 | 0.116 | 62.6 | 7.9 | 0.80 | 13.9 | 0.00167 | 3.06 | 27.7 | 59.3 | 600.3 |
| 1.26 | 1.34 | 0.112 | 0.117 | 127.8 | 11.3 | 0.76 | 20.9 | 0.00167 | 3.11 | 27.2 | 59.3 | 600.4 |
| 1.72 | 1.80 | 0.112 | 0.116 | 238.6 | 15.4 | 0.74 | 28.1 | 0.00166 | 3.19 | 26.4 | 59.3 | 600.8 |
| 2.32 | 2.22 | 0.112 | 0.113 | 430.6 | 20.8 | 0.73 | 34.6 | 0.00167 | 3.20 | 26.1 | 59.3 | 600.5 |
| 0.23 | 0.31 | 0.065 | 0.068 | 12.8 | 3.6 | 0.87 | 4.1 | 0.00048 | 3.21 | 115.3 | 70.3 | 2100.7 |
| 0.33 | 0.33 | 0.068 | 0.070 | 24.2 | 4.9 | 0.30 | 4.8 | 0.00056 | 5.26 | 72.1 | 64.3 | 1777.8 |
| 0.65 | 0.72 | 0.094 | 0.096 | 47.4 | 6.9 | 0.53 | 10.7 | 0.00111 | 3.87 | 98.1 | 62.3 | 900.9 |
| 0.58 | 0.50 | 0.090 | 0.100 | 41.7 | 6.5 | 0.37 | 6.4 | 0.00088 | 5.00 | 69.4 | 72.4 | 1139.5 |
| 0.68 | 0.53 | 0.096 | 0.097 | 50.0 | 7.1 | 0.71 | 6.6 | 0.00098 | 3.64 | 101.2 | 74.4 | 1020.8 |
| 0.62 | 0.54 | 0.075 | 0.078 | 67.1 | 8.2 | 0.71 | 7.1 | 0.00064 | 3.55 | 98.8 | 70.3 | 1571.6 |
| 0.46 | 0.48 | 0.080 | 0.085 | 33.6 | 5.8 | 1.59 | 6.3 | 0.00071 | 2.37 | 113.2 | 70.3 | 1410.0 |
| 2.55 | 2.37 | 0.101 | 0.104 | 637.0 | 25.2 | 0.97 | 32.1 | 0.00118 | 2.99 | 106.0 | 68.3 | 850.5 |
| 3.91 | 3.53 | 0.438 | 0.445 | 79.5 | 8.9 | 2.13 | 47.8 | 0.02210 | 2.02 | 163.1 | 68.3 | 45.2 |
| 2.87 | 2.87 | 0.368 | 0.383 | 60.7 | 7.8 | 2.58 | 41.3 | 0.01654 | 1.78 | 180.3 | 64.3 | 60.5 |
| 15.48 | 15.38 | 0.751 | 0.824 | 425.1 | 20.6 | 1.81 | 208.1 | 0.06536 | 2.18 | 166.0 | 68.3 | 15.3 |
| 30.58 | 28.41 | 0.914 | 1.012 | 1118.6 | 33.4 | 1.78 | 384.3 | 0.09709 | 2.20 | 165.9 | 68.3 | 10.3 |
| 1.52 | 1.36 | 0.256 | 0.275 | 35.2 | 5.9 | 0.80 | 20.2 | 0.00831 | 3.15 | 115.8 | 62.3 | 120.4 |
| 2.70 | 2.71 | 0.511 | 0.546 | 28.0 | 5.3 | 0.76 | 40.2 | 0.03295 | 3.22 | 115.6 | 62.3 | 30.3 |
| 4.65 | 4.67 | 0.622 | 0.690 | 55.8 | 7.5 | 0.74 | 69.3 | 0.04902 | 3.26 | 115.2 | 62.3 | 20.4 |
| 25.20 | 24.51 | 0.880 | 0.955 | 820.1 | 28.6 | 1.69 | 363.6 | 0.09851 | 2.16 | 164.8 | 62.3 | 10.2 |
| 29.46 | 28.49 | 0.655 | 0.707 | 2020.0 | 44.9 | 0.55 | 385.4 | 0.04951 | 3.99 | 77.9 | 68.3 | 20.2 |
| 25.67 | 24.36 | 0.885 | 0.859 | 840.4 | 29.0 | 0.95 | 350.1 | 0.09616 | 2.92 | 120.0 | 64.3 | 10.4 |
| 34.50 | 32.95 | 0.466 | 0.478 | 5477.9 | 74.0 | 0.95 | 445.8 | 0.02506 | 3.02 | 85.4 | 68.3 | 39.9 |
| 32.99 | 33.90 | 0.895 | 0.924 | 1358.8 | 36.9 | 0.67 | 487.2 | 0.09852 | 3.47 | 108.7 | 64.3 | 10.2 |
| 3.31 | 2.61 | 0.716 | 0.785 | 21.4 | 4.6 | 1.03 | 40.1 | 0.06712 | 2.73 | 131.7 | 60.3 | 14.9 |
| 5.40 | 5.43 | 0.349 | 0.355 | 239.2 | 15.5 | 0.76 | 86.2 | 0.01650 | 3.11 | 26.7 | 58.3 | 60.6 |
| 10.82 | 10.91 | 0.350 | 0.363 | 956.1 | 30.9 | 0.76 | 173.1 | 0.01654 | 3.12 | 26.6 | 58.3 | 60.4 |
| 17.09 | 16.49 | 0.350 | 0.352 | 2387.0 | 48.9 | 0.77 | 261.4 | 0.01653 | 3.09 | 26.7 | 58.3 | 60.5 |
| 22.62 | 22.09 | 0.350 | 0.368 | 4179.2 | 64.6 | 0.77 | 350.3 | 0.01656 | 3.10 | 26.6 | 58.3 | 60.4 |
| 0.26 | 0.19 | 0.060 | 0.064 | 19.2 | 4.4 | 1.19 | 7.0 | 0.00111 | 1.66 | 313.1 | 69.4 | 900.6 |
| 12.72 | 12.89 | 0.564 | 0.625 | 509.4 | 22.6 | 0.90 | 462.4 | 0.09708 | 1.90 | 270.7 | 69.4 | 10.3 |

# References


(1) Simmert, S.; Abdosamadi, M. K.; Hermsdorf, G.; Schäffer, E. LED-based interference-reflection microscopy combined with optical tweezers for quantitative three-dimensional microtubule imaging. *Opt. Express* **2018**, *26*, 14499–14513.

(2) Mahamdeh, M.; Simmert, S.; Luchniak, A.; Schäffer, E.; Howard, J. Label-free high-speed wide-field imaging of single microtubules using interference reflection microscopy. *J. Micros.* **2018**, *272*, 60–66.

(3) Sudhakar, S.; Abdosamadi, M. K.; Jachowski, T. J.; Bugiel, M.; Jannasch, A.; Schäffer, E. Germanium nanospheres for ultraresolution picotensiometry of kinesin motors. *Science* **2021**, *371*, eabd9944.

(4) Mahamdeh, M.; Schäffer, E. Optical tweezers with millikelvin precision of temperature-controlled objectives and base-pair resolution. *Opt. Express* **2009**, *17*, 17190–17199.

(5) Hermsdorf, G. L.; Szilagyi, S. A.; Rösch, S.; Schäffer, E. High performance passive vibration isolation system for optical tables using six-degree-of-freedom viscous damping combined with steel springs. *Rev. Sci. Instrum.* **2019**, *90*, 015113.

(6) Tolić-Nørrelykke, S. F.; Schäffer, E.; Howard, J.; Pavone, F. S.; Jülicher, F.; Flyvbjerg, H. Calibration of optical tweezers with positional detection in the back focal plane. *Rev. Sci. Instrum.* **2006**, *77*, 103101.

(7) Hinamoto, T.; Hotta, S.; Sugimoto, H.; Fujii, M. Colloidal solutions of silicon nanospheres toward all-dielectric optical metafluids. *Nano Lett* **2020**, *20*, 7737–7743.

(8) Sugimoto, H.; Okazaki, T.; Fujii, M. Mie resonator color inks of monodispersed and perfectly spherical crystalline dilicon nanoparticles. *Adv. Optical Mater.* **2020**, *8*.

(9) Schäffer, E.; Nørrelykke, S. F.; Howard, J. Surface forces and drag coefficients of mi-

crospheres near a plane surface measured with optical tweezers. *Langmuir* **2007**, *23*, 3654–3665.

(10) Berg-Sørensen, K.; Flyvbjerg, H. Power spectrum analysis for optical tweezers. *Rev. Sci. Instrum.* **2004**, *75*, 594–612.

(11) Nørrelykke, S. F.; Flyvbjerg, H. Power spectrum analysis with least-squares fitting: Amplitude bias and its elimination, with application to optical tweezers and atomic force microscope cantilevers. *Rev. Sci. Instrum.* **2010**, *81*, 075103.

(12) Simmert, S.; Jachowski, T. A Python package to calibrate optical tweezers and analyze time-dependent signals. figshare (2020), `https://github.com/cellular-nanoscience/pyotic`.

(13) Pollard, M. R.; Botchway, S. W.; Chichkov, B.; Freeman, E.; Halsall, R. N. J.; Jenkins, D. W. K.; Loader, I.; Ovsianikov, A.; Parker, A. W.; Stevens, R.; Turchetta, R.; Ward, A. D.; Towrie, M. Optically trapped probes with nanometer-scale tips for femto-Newton force measurement. *New J. Phys.* **2010**, *12*, 113056.

(14) Adriana, F.; Selma, G.; Archimedes, J., B. de Castro; Vivaldo, M. N.; Liliana de, Y. P.; Gustavo, P. M.; Luiz, C. B.; Carlos, L. C. Determination of femto Newton forces and fluid viscosity using optical tweezers: application to Leishmania amazonensis. *Proc. SPIE* **2005**, *5699*, 419–425.

(15) Hohng, S.; Zhou, R.; Nahas, M. K.; Yu, J.; Schulten, K.; Lilley, D. M. J.; Ha, T. Fluorescence-force spectroscopy maps two-dimensional reaction landscape of the Holliday junction. *Science* **2007**, *318*, 279–283.

(16) Rohrbach, A. Switching and measuring a force of 25 femtoNewtons with an optical trap. *Opt. Express* **2005**, *13*, 9695–9701.

(17) Imasato, H.; Yamakawa, T. Measurement of dielectrophoretic force by employing controllable gravitational force. *J. Electrophor.* **2008**, *52*, 1–8.

(18) Helden, L.; Eichhorn, R.; Bechinger, C. Direct measurement of thermophoretic forces. *Soft Matter* **2015**, *11*, 2379–2386.

(19) Gibson, G. M.; Leach, J.; Keen, S.; Wright, A. J.; Padgett, M. J. Measuring the accuracy of particle position and force in optical tweezers using high-speed video microscopy. *Opt. Express* **2008**, *16*, 14561–14570.

(20) Rudhardt, D.; Bechinger, C.; Leiderer, P. Repulsive depletion interactions in colloid-polymer mixtures. *J. Phys.: Condens. Matter* **1999**, *11*, 10073.

(21) Stoev, I. D.; Seelbinder, B.; Erben, E.; Maghelli, N.; Kreysing, M. Highly sensitive force measurements in an optically generated, harmonic hydrodynamic trap. *eLight* **2021**, *1*, 2662–8643.

(22) Prieve, D. C. Measurement of colloidal forces with TIRM. *Adv. Colloid Interface Sci.* **1999**, *82*, 93 – 125.

(23) Maragò, O. M.; Jones, P. H.; Bonaccorso, F.; Scardaci, V.; Gucciardi, P. G.; Rozhin, A. G.; Ferrari, A. C. Femtonewton force sensing with optically trapped nanotubes. *Nano Lett.* **2008**, *8*, 3211–3216.

(24) Chen, F.-J.; Wong, J.-S.; Hsu, K. Y.; Hsu, L. Thermally activated state transition technique for femto-Newton-level force measurement. *Opt. Lett.* **2012**, *37*, 1469–1471.

(25) Sainis, S. K.; Germain, V.; Mejean, C. O.; Dufresne, E. R. Electrostatic interactions of colloidal particles in nonpolar solvents: role of surface chemistry and charge control agents. *Langmuir* **2008**, *24*, 1879–3088.

(26) Zensen, C.; Villadsen, N.; Winterer, F.; Keiding, S. R.; Lohmüller, T. Pushing nanoparticles with light — A femtonewton resolved measurement of optical scattering forces. *APL Photonics* **2016**, *1*, 026102.

(27) Liu, L.; Kheifets, S.; Ginis, V.; Capasso, F. Subfemtonewton force spectroscopy at the thermal limit in liquids. *Phys. Rev. Lett.* **2016**, *116*, 228001.

(28) Shan, X.; Ding, L.; Wang, D.; Wen, S.; Shi, J.; Chen, C.; et all., Sub-femtonewton force sensing in solution by super-resolved photonic force microscopy. *Nat. Photonics* **2024**, *8*, 3211–3216.